

## Article

# Adaptive Design of Solar-Powered Energy Systems Based on Daily Clearness State Evolution

Dong Liang <sup>1,\*</sup>, Long Ma <sup>1</sup>, Peng Wang <sup>1</sup>, Yuanxia Li <sup>1</sup> and Yiping Luo <sup>2</sup>

<sup>1</sup> State Grid Gansu Electric Power Company Linxia Power Supply Company, Linxia 731100, China; qiongma2022@163.com (L.M.); wzuohao@163.com (P.W.); shangzpz0829@163.com (Y.L.)

<sup>2</sup> State Key Laboratory of Eco-Hydraulic in Northwest Arid Region, Xi'an University of Technology, Xi'an 710048, China; luoyiping1117@163.com

\* Correspondence: liangdong0310@163.com

**Abstract:** The optimal designing of the hybrid energy system (HES) is a challenging task due to the multiple objectives and various uncertainties. Especially for HES, primarily powered by solar energy, the reference solar radiation data directly impact the result of the optimization design. To incorporate the stochastic characteristics of solar radiation into the sizing process, a data-driven stochastic modeling method for solar radiation is proposed. The method involves two layers of stochastic processes that capture the intraday variation and daily evolution of solar radiation. First, the clearness index (CI) is introduced to describe the radiation intensity at different times. Then, the daily clearness state (DCS) is proposed, based on the statistical indicators of the intraday CI. The Markov model is used to describe the stochastic evolutionary characteristics between different DCSs. The probabilistic distribution of the CI under different DCS is obtained based on the diffusion kernel density estimation (DKDE), which is used for the stochastic generation of the CI at various times of the day. Finally, the radiation profile required for the optimal design is obtained by the stochastic generation of the DCS sequences and the intraday clearness index under corresponding states. A case study of an off-grid solar-powered HES is provided to illustrate this methodology.

**Keywords:** solar radiation; hybrid energy system; optimal design; Markov model; diffusion-based kernel density estimation



**Citation:** Liang, D.; Ma, L.; Wang, P.; Li, Y.; Luo, Y. Adaptive Design of Solar-Powered Energy Systems Based on Daily Clearness State Evolution. *Energies* **2024**, *17*, 2328. <https://doi.org/10.3390/en17102328>

Academic Editor: Jesús Polo

Received: 27 March 2024

Revised: 4 May 2024

Accepted: 9 May 2024

Published: 11 May 2024



**Copyright:** © 2024 by the authors. Licensee MDPI, Basel, Switzerland. This article is an open access article distributed under the terms and conditions of the Creative Commons Attribution (CC BY) license (<https://creativecommons.org/licenses/by/4.0/>).

## 1. Introduction

The global drive towards environmental protection and energy sustainability has led to the increasing deployment of hybrid energy systems (HESs), which leverage the complementarity of various energy sources to improve system performance and enable the integration of renewable energy sources [1–4]. Among these, photovoltaic (PV) systems have emerged as a leading technology, with rapidly decreasing costs and maturing auxiliary devices contributing to explosive growth in the global installed capacity [5–7]. However, the inherent uncertainty of solar power poses significant challenges to the photovoltaic-based HESs, particularly in the optimal design phase, when the predictive information is hard to get, making it challenging to achieve an optimal configuration that balances load demand, minimizes cost, and meets other performance indices [8–10]. It is necessary to identify a reasonable method for the HES optimization design to quantitatively analyze the uncertainty of solar radiation.

In outdoor application scenarios, the uncertainty of solar power generation is caused by factors such as temperature, efficiency, and variations in the radiance received by the panel. Radiation is the direct source of solar energy, making it the main factor contributing to the volatility of PV systems. Typically, researchers construct physical models of PV modules to evaluate the effects of radiation changes on the final energy output of HES [11–14]. Radiation data is usually based on typical days (weeks, months, or years) or on historical measured sequences. While one could track the total global solar spectrum on

an inclined plane using satellite datasets [15], this approach may provide valuable insights into solar radiation dynamics, but it demands significant computational resources and data processing efforts. In addition, even if analytical methods potentially offer deterministic results for specific scenarios, they will not fully address the variability inherent in real-world HES conditions [16]. For example, optimizing HES includes complex interactions between multiple energy sources, diverse optimization objectives, and the need for comprehensive uncertainty-containing radiation information. Therefore, we opted for a stochastic modeling approach, which we integrated into our HES optimization framework. This helps provide complementary benefits in addressing uncertainties, thus improving decision-making effectiveness. To this end, some researchers use stochastic sampling to incorporate radiation uncertainty into the optimal design of HES [17]. Li et al. used Monte Carlo simulation and sensitivity analysis to quantify the uncertainties associated with the optimal design of solar heating systems [18]. Cho et al. used the scenario-based approach to represent solar radiation uncertainty and time variability in the optimal design of HES [19]. The scenarios are randomly chosen from twelve years of Typical Meteorological Year data. Liu proposed an uncertainty-based multi-objective design method by generating uncertainty distributions for load prediction and RESs production based on Monte Carlo simulation [20]. The impact of the degree of uncertainty and scenario settings was analyzed simultaneously.

In addition, another effective method for addressing radiation uncertainty is to generate simulate sequences using stochastic modeling of cloud cover [21]. The radiation outside of the atmosphere at any given location on earth can be determined based on its relative position to the sun. However, the radiation received on land is weakened due to atmospheric transmittance and induced fluctuation caused by stochastic cloud motion, and this rate varies dynamically as air mass and cloud motion change over time [22–24]. To describe various weather states, the clearness index is introduced and widely used in solar radiation stochastic modeling. Ngoko et al. proposed a probabilistic model for the synthetic generation of 1 min global solar radiation data based on the second-order Markov model [25]. The model was validated by confirming the reasonable agreement between the synthetic and observed datasets. Bouabdallah et al. simulated solar radiation with hour-level stochastic cloud cover sequences, which are generated based on Markov transition matrices (MTM) and used for the sizing optimization of stand-alone PV systems [26]. Although the studies mentioned above consider uncertain solar radiation sequences, for HES optimal design, the radiation must satisfy its rationality as random time series, which is expressed as the rational variation in daily and intraday radiation intensity. Few studies have considered both stochastic processes of the daily and intraday radiation transition, which directly determine the temporal change characteristics of the final radiation sequences.

In the present study, the daily clearness states (DCSs) are introduced, based on the intraday clearness index (CI) distribution, to describe the daily radiation intensity. The stochastic evolution characteristics in DCSs is then modeled using the Markov model. The obtained model is verified based on the Markov property and stationarity. Moreover, diffusion-based kernel density estimation (DKDE) is applied to fit the intraday CI distribution at different DCS. By integrating the two stochastic processes of the daily clearness states and the intraday clearness index, the stochastic model for solar radiation is established. A total number of 2000 radiation scenarios are generated for optimal sizing of an HES consisting of a PV, storage battery, and backup diesel generator. Half are used to solve the optimization problem, with the objective of minimizing the COE, to obtain the variation range of the optimal size of each component. The other half is used to perform a techno-economic analysis of the candidate size combinations to determine the final HES configuration.

This paper is organized as follows: Section 2 focuses on the stochastic modeling of solar radiation. The mathematical modeling of an off-grid PV-based HES is described in Section 3. Section 4 presents the results of the case study used to demonstrate our method. The conclusions are drawn in Section 5.

## 2. Stochastic Model Description

The total solar radiation  $G_{tot}$  received on the ground can be divided into three parts consisting of direct  $G_{dir}$ , diffused  $G_{dif}$ , and reflected  $G_r$  irradiation, as follows:

$$G_{tot} = G_{dir} + G_{dif} + G_r \quad (1)$$

The Hay–Davies–Klucher–Reindl (HDKR) anisotropic model provides a method that considers the effect of clouds on terrestrial radiation through the clearness index and the diffuse fraction. The clearness index is defined as the ratio between the solar radiation received on the horizontal surface  $G_h$  and the horizontal component of the extraterrestrial radiation  $G_0$ :

$$k_t = G_h / G_0 \quad (2)$$

The horizontal component of the extraterrestrial radiation  $G_0$  can be calculated as:

$$G_0 = G_{sc} [1 + 0.033 \cos(360^\circ N / 365)] \cos(\theta_z) \quad (3)$$

where  $\theta_z$  is the zenith angle,  $N$  is the  $N$ th day of the year, and  $G_{sc}$  is the solar constant, set to  $1367 \text{ W/m}^2$  in this paper. Note that there are minor fluctuations in the solar constant, primarily due to variations in solar activity, such as changes in the number and activity level of sunspots over the solar cycle [27]. While these variations may cause some fluctuations in the solar constant, they are relatively small and typically fall within acceptable ranges. Therefore, the solar constant is generally regarded as an approximately constant value.

A generic piecewise function of the diffuse fraction  $f(k_t)$  is proposed by Bouabdallah et al., expressed as [28]:

$$f(k_t) = \begin{cases} 1 - 0.13k_t, & k_t \leq 0.22 \\ 0.58 + 3.7k_t - 10.4k_t^2 + 6.4k_t^3, & 0.22 \leq k_t \leq 0.78 \\ 0.27 - 0.09k_t, & k_t > 0.78 \end{cases} \quad (4)$$

Then, the three components of the radiation can be expressed as:

$$G_{dir} = G_h [1 - f(k_t)] R_b \quad (5)$$

$$G_{dif} = G_h f(k_t) \left\{ A_i R_b + (1 - A_i) R_{dif} \left[ 1 + \sqrt{1 - f(k_t)} \sin^3(0.5\beta) \right] \right\} \quad (6)$$

$$G_r = \rho G_h R_r \quad (7)$$

where  $R_b$  is the ratio of direct radiation between the tilted and horizontal plane,  $R_{dif}$  is the tilt factor of the diffused component,  $R_r$  is the tilt factor for the reflected component,  $\rho$  is the albedo, and  $A_i$  is the anisotropic index. The detailed calculation process of the HDKR model can be found in the relative literature [29–31].

A dataset of one year of measured solar radiation is adopted in this paper, which was measured in Yulin, China, with a longitude of  $109.16^\circ \text{ E}$ , and a latitude of  $38.29^\circ \text{ N}$ . The measured radiation data covers a complete year from 1 January 2021 to 31 December 2021, with a time interval of 1 h, and was provided by the electric power department of Shaanxi Province, in which Yulin is located. The intention of the proposed stochastic model is to generate the stochastic CI sequence and then bring it into the HDKR model to obtain the corresponding  $G_{tot}$ . In this paper, the stochastic CI sequences are obtained by constructing daily and intraday stochastic models, which are based on Markov models and DKDE, respectively.

### 2.1. Daily Clearness State

A fundamental constraint in the optimal design of an energy system is the energy balance between supply and demand, as the daily radiation intensity transition will directly affect the size configuration. For instance, continuous daily low radiation increases the

potential PV capacity for more power generation. Therefore, the stochastic radiation sequences must consider the daily radiation intensity transition for an optimal design. As described in Equation (2), the clearness index represents the extent to which extraterrestrial radiation is attenuated by the atmosphere and clouds at a given time.

Considering this, the daily clearness states (DCSs) are introduced according to the intraday CIs distribution to represent the daily radiation intensity. The median of intraday CIs is used to classify DCSs, given its ability to reflect the concentrated trend and avoid the effects of extreme outliers. A total of nine DCSs are defined in this paper, uniformly distributed between 0 and 1, with a step of 0.1, as shown in Table 1. Note that intervals  $[0.8, 0.9]$  and  $[0.9, 1]$  both are classified as  $s_9$ , due to the existence of atmospheric transmittance, which will inevitably weaken the radiation received on the ground.

**Table 1.** Daily clearness state classification.

The Median of Intraday CIs	Daily Clearness State
$[0.0, 0.1]$	$s_1$
$[0.1, 0.2]$	$s_2$
...	...
$[0.7, 0.8]$	$s_8$
$[0.8, 1.0]$	$s_9$

Figure 1 shows the statistical information for the intraday clearness index (CI) values at different DCS, along with the corresponding normalized radiation curves. Note that the DCSs reflect the overall daily state of radiation intensity, independent of its intraday fluctuations. Although the range of intraday CIs in some states, like states 5 and 6, are dispersed and span multiple state intervals, the difference in radiation intensity can still be distinguished from the  $G_h$  area diagram. The dispersion of intraday CI values represents, to some extent, the fluctuating state of radiation, which is considered by the intraday CI stochastic model.

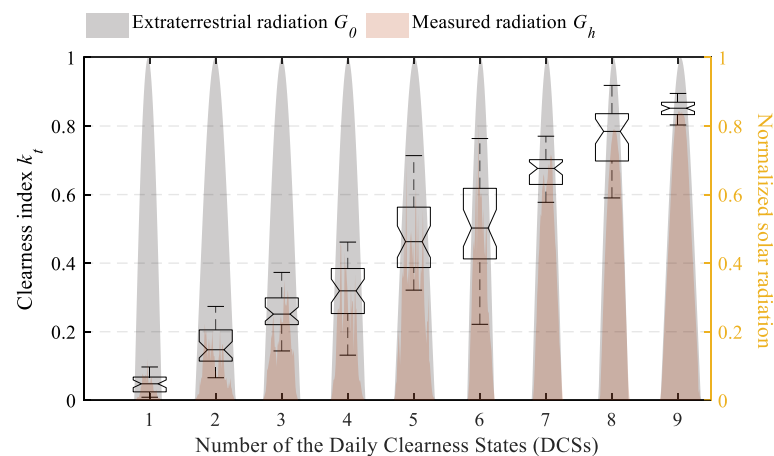


**Figure 1.** The boxplots of the clearness index at different daily clearness states and the normalized curve of corresponding extraterrestrial radiation and measured radiation.

## 2.2. State Transition Matrix

The Markov model is capable of describing the transition probability of a finite state in a stochastic process through the Markov transition matrices (MTMs). In general, weather-related parameters, including the DCS proposed in this paper, are highly complex and nonlinear, and do not fully conform to the Markov properties. However, in certain simplified models or specific circumstances, the transition of weather phenomena can be approximated as Markov processes, which has been applied and validated in many studies [24,25,32]. In this paper, the Markov model is employed for stochastic modeling of

the DCSs transition, which provides transition probabilities between any two DCSs, as illustrated in Figure 2. The frequency counting method is used to estimate the transition probabilities, based on observed frequencies of events in the historical dataset. Specifically, the estimated transition probability can be calculated by:

$$\hat{p}_{ij} = \frac{A_{ij}}{\sum_{j=1}^M A_{ij}} \tag{8}$$

where  $A_{ij}$  is the number of observed transitions from state  $i$  to state  $j$ ;  $M$  is the number of the states.

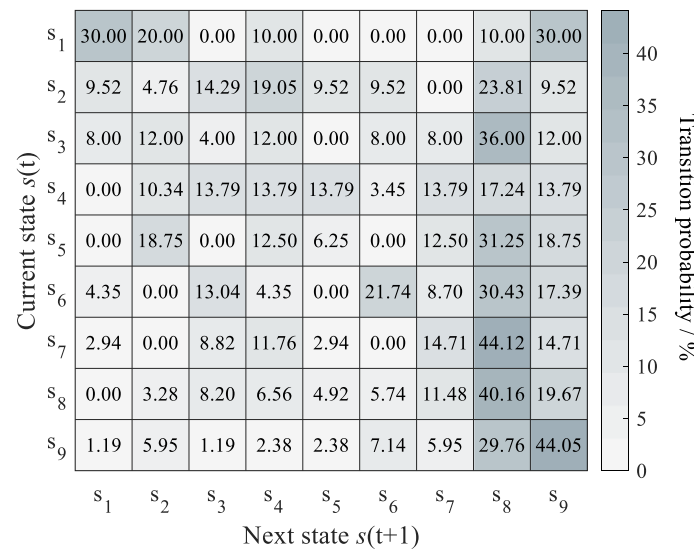


Figure 2. The Markov transition matrices (MTM) of the daily clearness states.

To ensure the validity of the model, the Markov chain property and stationarity of the DCS sequence must be statistically tested. The Markov chain properties can be evaluated by assessing the dependence of successive events. Based on the null hypothesis that successive events are independent, the statistic  $\alpha$  is asymptotically distributed as  $\chi^2$ , with  $(N - 1)^2$  degrees of freedom. This statistic is defined as:

$$\alpha = 2 \sum_{i,j}^N n_{ij} \ln(p_{ij} / p_j) \tag{9}$$

where  $N$  is the total number of states, and  $n_{ij}$  and  $p_{ij}$  are the frequency and probability of state  $j$  transfer from state  $i$ , respectively.

If the transition probabilities of a Markov process remain independent over time, the process is considered stationary, and the statistic  $\beta$  has a  $\chi^2$  distribution with  $N(N - 1)(T - 1)$  degrees of freedom.

$$\beta = 2 \sum_t^T \sum_{i,j}^N n_{ij}(t) \ln[p_{ij}(t) / p_{ij}] \tag{10}$$

where  $T$  is the number of subintervals and is set to four here. Each subinterval represents about one season of the total 365 days.

As summarized in Table 2, the value of  $\alpha$  is larger than the  $\chi^2$ , with 64 df at the 5% level, which means we can reject the null hypothesis and conclude that the transition of DCS possesses the first-order Markov chain property. Meanwhile, the stationary property has been proven, as the value of  $\beta$  is smaller than the  $\chi^2$  at the 5% level, with 216 df.

**Table 2.** Markov chain property and stationarity.

$\alpha$	$\chi^2$ with 64 df	$\beta$	$\chi^2$ with 216 df
284.7373	83.6753	216.4788	251.2864

Figure 3 shows the construction method for the DCS sequences, where  $v$  refers to random variables uniformly distributed in the interval  $[0, 1]$ , and  $p$  is the corresponding transition probability from the obtained Markov transition matrices. Note that the probability vector used on the first day is calculated by the stationary distribution of the proposed Markov model. For the rest of the sequence, the probability vector is the corresponding transition vector of the previous state.

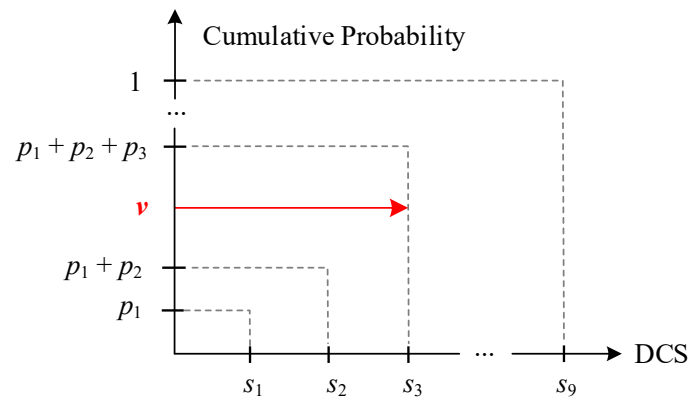


**Figure 3.** Construction method of the DCS sequences using the Markov model, and the red arrow highlights the DCS corresponding to the stochastic variable  $v$ .

2.3. Distribution Fitting of Intraday CIs

The CIs at each time of the day are treated as stochastic variables, satisfying a certain distribution that can be fitted based on the CI sets at different DCSs from the samples. The diffusion-based kernel density estimator (DKDE) has been shown to be superior in distribution fitting, as it addresses traditional KDE concerns regarding boundary bias and optimal bandwidth, while also improving computational speed [33–35].

Given one-dimensional  $n$  sample feature space  $\{x_1, x_2, \dots, x_n\}$ , the estimated probability density function (PDF) obtained by KDE is:

$$\hat{f}(x, w) = \frac{1}{nw} \sum_{i=1}^n K\left(\frac{x - x_i}{w}\right) \tag{11}$$

where  $K(\cdot)$  is the kernel function, and  $w$  is the bandwidth.

The Gaussian kernel function is commonly used in KDE, which can be expressed as:

$$\phi(x) = \frac{1}{\sqrt{2\pi}} e^{-\frac{1}{2}x^2} \tag{12}$$

The Gaussian kernel density estimator (GKDE) is the only solution to the diffusion partial differential equation, as shown in Equation (12).

$$\frac{\partial}{\partial t} \hat{f}(x; t) = \frac{1}{2} \frac{\partial^2}{\partial x^2} \hat{f}(x; t), x \in R, t > 0 \tag{13}$$

By defining the domain  $R$  belong to  $[0, 1]$ , the initial and boundary condition can be expressed as:

$$\hat{f}(x, 0) = \frac{1}{n} \sum_{i=1}^n \delta(x - x_i) \tag{14}$$

$$\frac{\partial}{\partial x} \hat{f}(x; t) \Big|_{x=0} = \frac{\partial}{\partial x} \hat{f}(x; t) \Big|_{x=1} = 0 \tag{15}$$

where  $\delta(\cdot)$  is Dirac function.

Substituting the CI sets under each DCS, the estimated PDFs can be obtained by solving the diffusion partial differential equation in Equation (12). The obtained PDFs and corresponding CDFs by DKDE at different DCSs are shown in Figure 4. Due to the uniform [0, 1] property of the CDF, the stochastic CI can be obtained from the inverse CDF by generating a random variable of uniform [0, 1], as shown in Equation (15).

$$\hat{k}_t = F_i^{-1}(v), \quad i = 1, 2, \dots, N \tag{16}$$

where  $v$  is the random variable, and  $F_i$  is the CDF at  $i$ -th DCS.

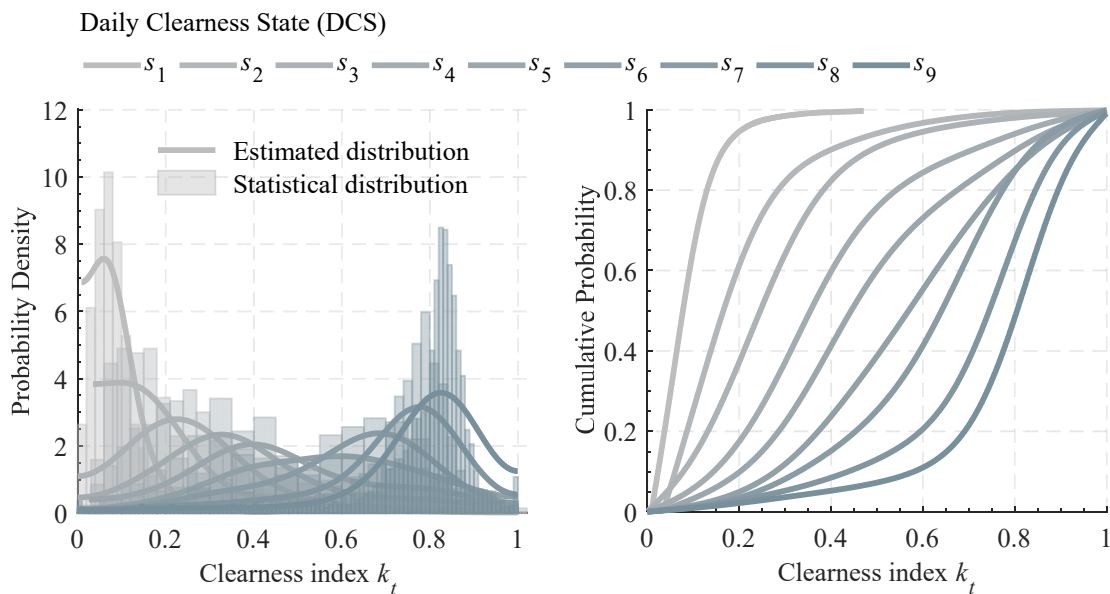


**Figure 4.** The estimated PDFs and CDFs of the clearness index at different daily clearness states.

#### 2.4. Stochastic Solar Radiation

The final solar radiation sequences are determined by generating stochastic DCS transition chains, with their corresponding intraday CIs. Figure 5 shows an annual hourly stochastic solar radiation curve; as the stochastic model is based on a clear-sky model, the simulated radiation data changes are consistent with the quarterly trend.

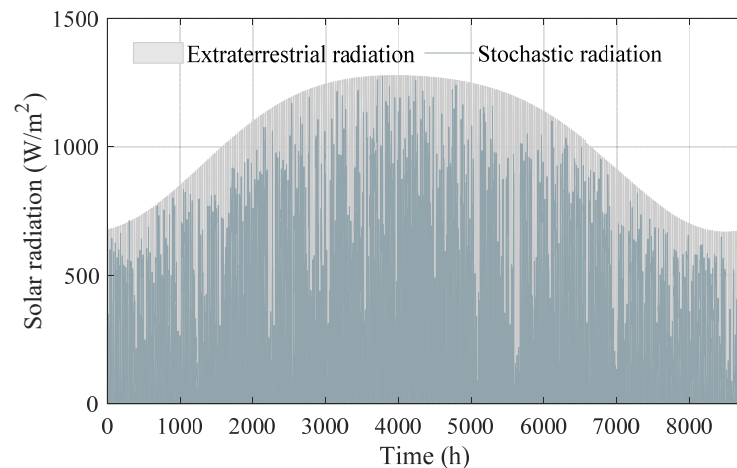


**Figure 5.** Simulated stochastic solar radiation.

### 3. Optimization Model of HES

The optimal design of a residential off-grid photovoltaic-based HES is used to illustrate the methodology proposed in this paper. The configuration of the hybrid system, as shown in Figure 6, comprises a PV-battery system with a backup diesel generator. This configuration is particularly useful for remote areas where the grid is difficult to reach, and solar power is sufficient. The battery smooths out fluctuation in the PV output and improves the efficiency of the system, with a backup diesel generator ensuring an uninterrupted power supply.

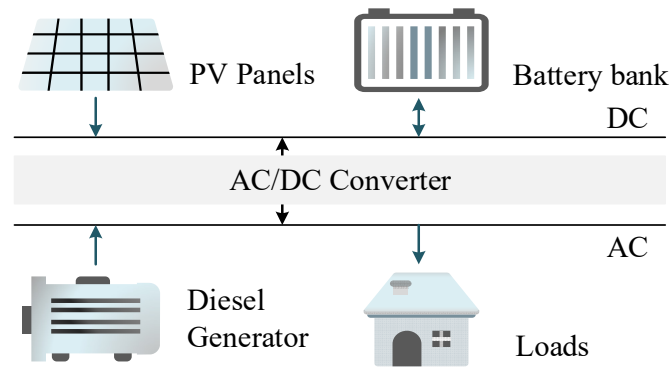


Figure 6. Configuration of the hybrid system.

#### 3.1. Objective Function

The cost of the energy (COE) is used to evaluate the performance of the HES configuration, which is usually composed of equipment depreciation cost  $C^{dep}$ , fuel cost  $C^{fuel}$ , emission cost  $C^{emi}$ , maintenance cost  $C^{mai}$ , and auxiliary equipment depreciation  $C_{aux}^{dep}$  in terms of the per unit energy converted to load demand.

$$COE = \frac{\sum_{t=1}^T \sum_{i=1}^I (C_{i,t}^{dep} + C_{i,t}^{emi} + C_{i,t}^{fuel}) + C_{aux}^{dep} + C^{mai}}{\sum_{t=1}^T d_t} \quad (17)$$

where  $T$  is the number of discretized times,  $I$  is the number of components in the proposed system, and  $d$  is the load demands.

The depreciation cost can be calculated from two aspects: the life lost over time (physical time) and the life lost due to operation (lifetime throughput), which can be expressed by Equations (17) and (18), respectively.

$$C_{phy}^{dep} = wc^{cap} \frac{\Delta t}{t^{phy}} \quad (18)$$

$$C_{op}^{dep} = wc^{cap} \frac{p}{p^{life}} \quad (19)$$

where  $w$  is size of the component; note that the units of  $w$  for each component in this paper are kW, kWh, and  $m^2$ , corresponding to diesel generator, battery, and PV, respectively.  $\Delta t$  is the time step,  $c^{cap}$  is the cost of the per unit size of the component,  $t^{phy}$  is the physical lifetime,  $p$  is the energy supply from the component per time step, and  $p^{life}$  represents the energy lifetime throughput of the component.

Considering the time overlap, the depreciation cost at each time is set as the higher value between the two methods.

$$C^{dep} = \max(C_{phy}^{dep}, C_{op}^{dep}) \quad (20)$$

The fuel cost is determined as:

$$C^{fuel} = c^{fuel} \frac{p}{q_v \eta} \tag{21}$$

where  $c^{fuel}$  is the fuel price,  $q_v$  is the heat value of the fuel, and  $\eta$  refer to the efficiency.

In this paper, the cost of emission only considers the damage caused by the CO<sub>2</sub>, which can be calculated by the following equation:

$$C^{emi} = c_{CO_2}^{emi} f_{CO_2}^{emi} \frac{p}{\eta} \tag{22}$$

where  $c_{CO_2}^{emi}$  is the emission cost of the CO<sub>2</sub> per kilogram, and  $f_{CO_2}^{emi}$  is the emission factor.

To simplify the complexity of the model, the auxiliary equipment depreciation cost is assumed to be calculated based on the initial investment cost.

$$C_{aux}^{dep} = f_{aux}^{dep} \sum_{i=1}^I (w_i c_i^{cap}) \tag{23}$$

where  $f_{aux}^{dep}$  is the depreciate coefficient of the auxiliary equipment.

The optimal design of the HES aims to find the size configuration to meet the power demand with the lowest COE within a given timeframe. The final optimization objective can be written as:

$$\min \left\{ \frac{\sum_{t=1}^T \sum_{i=1}^I \left[ \max(C_{phy(i,t)}^{dep}, C_{op(i,t)}^{dep}) + C_{i,t}^{emi} + C_{i,t}^{fuel} \right] + C_{aux}^{dep} + C^{mai}}{\sum_{t=1}^T d_t} \right\} \tag{24}$$

### 3.2. Constraints

The HES should satisfy the energy balance constraint between energy supply and demand:

$$\sum_{i=1}^I p_{i,t} = d_t \text{ where } t = 1, 2, \dots, T \tag{25}$$

where  $p_{i,t}$  represent the power generation of component  $i$  at time  $t$ , and  $d_t$  is the power demand at time  $t$ .

The energy supply of each component needs to meet its capacity constraints:

$$\begin{cases} 0 \leq p_{DG,t} \leq w_{DG} \Delta t \\ 0 \leq p_{PV,t} \leq \eta_{PV} R_t w_{PV} \Delta t \\ 0 \leq p_{BT,t} \leq \min(V_{MAX}^{discharge} I_{MAX}^{discharge} \Delta t, w_{BT} \eta_{BT}^{discharge}) \\ 0 \geq p_{BT,t} \geq \max(-V_{MAX}^{charge} I_{MAX}^{charge} \Delta t, -w_{BT} / \eta_{BT}^{charge}) \end{cases} \tag{26}$$

For the battery, the constraints of state of charge (SOC) should also be satisfied, which can be expressed as:

$$\begin{cases} 0 \leq SOC_t = SOC_{t-1} + \frac{p_{BT,t}}{\eta_{BT}^{discharge} w_{BT}} \leq 1 \\ 0 \leq SOC_t = SOC_{t-1} + \frac{\eta_{BT}^{charge} p_{BT,t}}{w_{BT}} \leq 1 \end{cases} \tag{27}$$

Note that the depreciation cost is represented as a maximum value function; an auxiliary variable is set to linearize this as:

$$\left\{ \begin{array}{l} z \geq x \\ z \geq y \\ z \leq x + M(1 - u_1) \\ z \leq y + M(1 - u_2) \\ u_1 + u_2 \geq 1 \\ u_1, u_2 \in \{0, 1\} \end{array} \right. \quad (28)$$

where  $z$  is the auxiliary variable,  $x$  and  $y$  refer to the life lost over time and the life lost due to operation, respectively;  $M$  is a sufficiently large constant.

#### 4. Experimental Results

A total of 2000 sets of annual hourly stochastic solar radiation scenarios are generated by the proposed stochastic model. The data are equally divided into two blocks of 1000 sets, with half used for the optimal design of the proposed HES and the other half used for analysis of operational performance of the candidate sizes. The size of the PV panel, diesel generator, and battery are treated as decision variables in the optimal design process. The optimization models are solved using the Python 3.9 optimization package RSOME with Gurobi version 10.0.

The load profiles are randomly generated based on the typical load profile for a local village at the same location as the solar radiation data. Note that the study area consists of the simple hybrid energy systems of remote mountain villages. Their loads are mainly determined by essential production and living needs, and fluctuations due to changes in seasons, temperatures, etc., are typically small. Figure 7 illustrates the typical load profile, and the load variation rate is set as 0.2.

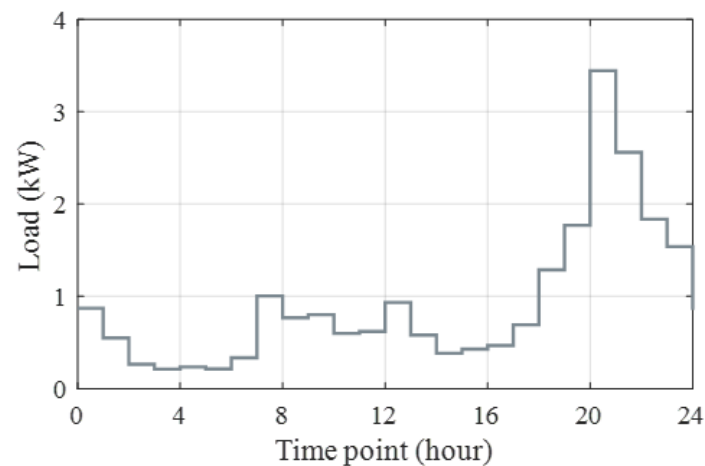


**Figure 7.** Daily typical load profile of the local village.

Technical data employed in the computations are provided in Table 3. These data cover the efficiency of each component, the costs, and other necessary parameters for the calculation process. Note that the estimates of some parameters may deviate from the actual scenarios, which, due to the costs, efficiency, reliability, and durability of the system devices, are intricately linked to their origin, manufacturer, and the current stage of development. Additionally, prices often include not only the cost of the equipment itself, but also the associated expenses, such as those related to installation and transportation, especially for the remote rural household users studied in this paper. The results obtained from the proposed optimization model only represent the optimal configuration under the set conditions. However, this framework is universal and replicable.

**Table 3.** Technical data employed in the computations.

Components	Description	Data	Source
PV array	Capital cost	USD 285.3/m <sup>2</sup>	e
	Efficiency	17.12%	[7]
	Lifetime	20 years	a
Diesel generator	Capital cost	USD 405.82/kW	[13]
	Efficiency	0.3	e
	Fuel price	USD 1.29/L	e
	Lifetime	15 years (or 50,000 operation hour)	a
	Emission factor	$7.05 \times 10^{-5}$ kg/kJ	e
Battery	Capital cost	USD 135.8/kWh	[11]
	Life cycles	1200	a
	Lifetime	10 years	a
	Maximum charge rate	0.3 C	e
	Maximum discharge rate	3 C	e
	Minimum state-of-charge	0.4	e
	Charge efficiency	0.9	e
	Discharge efficiency	0.9	e
Others	Load variation	0.2	a
	System maintenance cost	USD 0.015/h	a
	Auxiliary equipment cost	30% of initial capital cost	a
	System lifetime	15 years	a

Note: a—assumed values; e—estimated values.

Battery aging paths are determined by nonlinear functions of the state of charge (SOC), depth of discharge (DOD), C-rate (defined as the charge or discharge current divided by the battery's capacity to store an electrical charge, with the unit  $h - 1$ ), temperature, etc. Commonly, battery aging models adopted in microgrid assessment and control references are mainly simplified to be linearly related with DOD and cycle amounts [36]. In this paper, we have separately defined the lifetime and life cycles of the battery, representing the lifespan under standby conditions and its cycle lifespan, respectively.

The cost of auxiliary equipment depreciation, including the system controller, battery chargers, enclosures, switch gear, fuses, wiring, etc., was taken into account in the calculation. Note that the cost of the inverter, a key component of the HES, is not explicitly calculated in the optimization model, but is considered along with the cost of the auxiliary equipment. As a matter of fact, the selection of inverters is directly related to the capacity of the generating devices; once the capacity of generating devices is determined, compatible inverters can be determined. The cost of emissions was also considered; this is the responsibility of the user and is not always considered in some countries.

#### 4.1. Optimal Sizing

The time horizon of one year is chosen for the optimal design of the HES, as it encompasses a full cycle of solar motion. The results of the optimization are summarized in Figure 8, which shows a clear correspondence between the yearly total radiation and the annual COE. Specifically, the optimal sizing of the HES tends to involve a larger battery and a smaller diesel generator capacity for scenarios with higher yearly total radiation, resulting in a smaller annual COE. Conversely, scenarios with lower yearly total radiation require a larger diesel generator capacity to meet the load demand, resulting in a higher annual COE. The maximum and minimum yearly total radiation are 1874.6 kW/m<sup>2</sup> and 1607.4kW/m<sup>2</sup>, resulting in a difference of 14.25%, which corresponds to a COE of USD 0.372/kWh and USD 0.388/kWh, respectively, which represents a difference of 4.3%. This result underscores the sensitivity of the optimal sizing of the HES to variations in yearly total radiation levels and highlights the importance of the radiation uncertainty in the design of HES. Meanwhile, the optimal sizes in different radiation scenarios are maintained within a certain range, with PV in [10.58, 13.86] m<sup>2</sup>, battery in [7.3, 15.1] kWh, and diesel generator in [1.54, 2.22] kW.

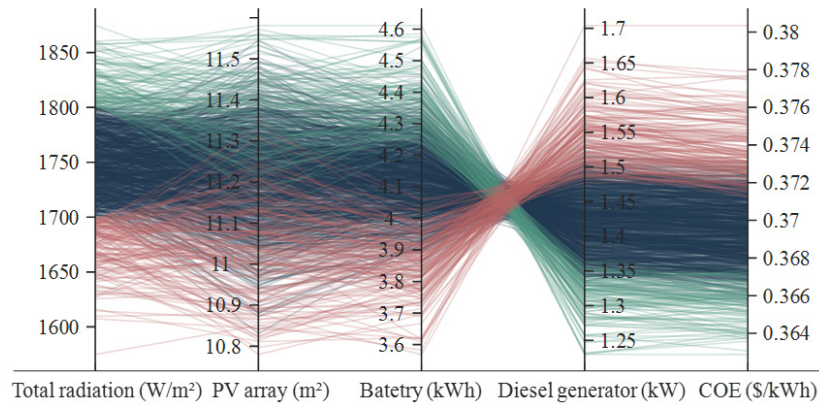


**Figure 8.** Results of the optimal design with stochastic radiation.

Additionally, the obtained operation schedule for each component in the HES over the entire simulation period is the optimal scheduling strategy for minimizing the COE. Figure 9 shows an example of the power dispatch schedule, with two time periods taken from winter and summer, respectively. The scenario of the example has the max yearly total radiation of 1874.6 kW/m<sup>2</sup>, with the sizes of PV of 13.07 m<sup>2</sup>, battery of 14.51 kWh, and diesel generator of 1.67 kW, resulting in an annual COE of USD 0.372/kWh.

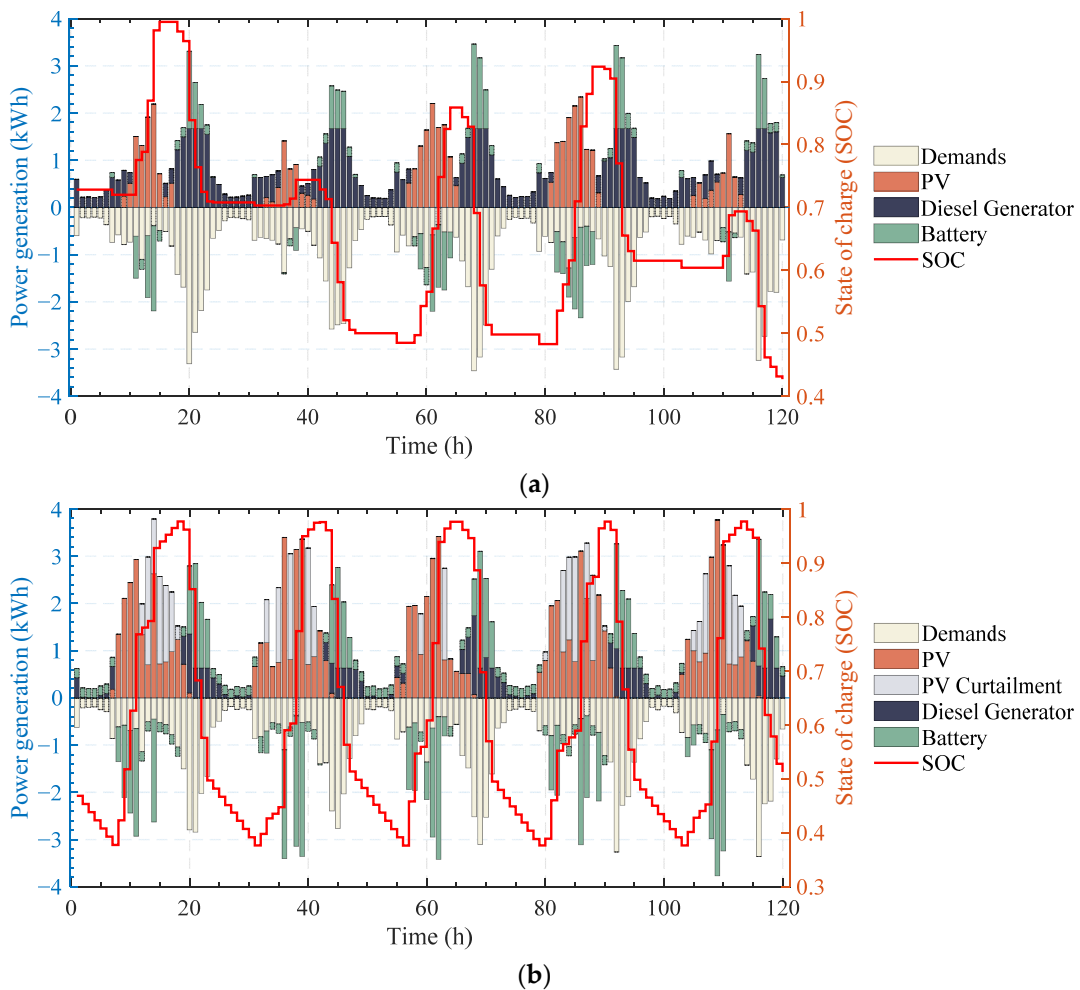


**Figure 9.** The power dispatch schedule of the optimal size under the scenario with yearly total radiation is 1874.6 kW/m<sup>2</sup>. (a) January 1st to 5th; (b) July 1st to 5th.

From Figure 9, as the demand is low during the daytime and high after sunset; excess power generated by the PV panel is stored in batteries and used along with the diesel generators for the night load. In the winter, the low intensity of solar radiation makes it necessary to combine with a diesel generator to meet the load supply during the daytime. Conversely, during the summer months, the increased generation of solar power allows for greater flexibility in the deployment of energy storage, resulting in a reduced reliance on diesel generators. As shown in Figure 9b, sufficient PV power generation causes the battery to undergo a full charge/discharge cycle per day, within the feasible SOC. Additionally, it is worth noting that during the winter months, all the PV power is utilized for the load supply or battery charge, whereas there is PV power curtailment during the summer months.

#### 4.2. Techno-Economic Analysis

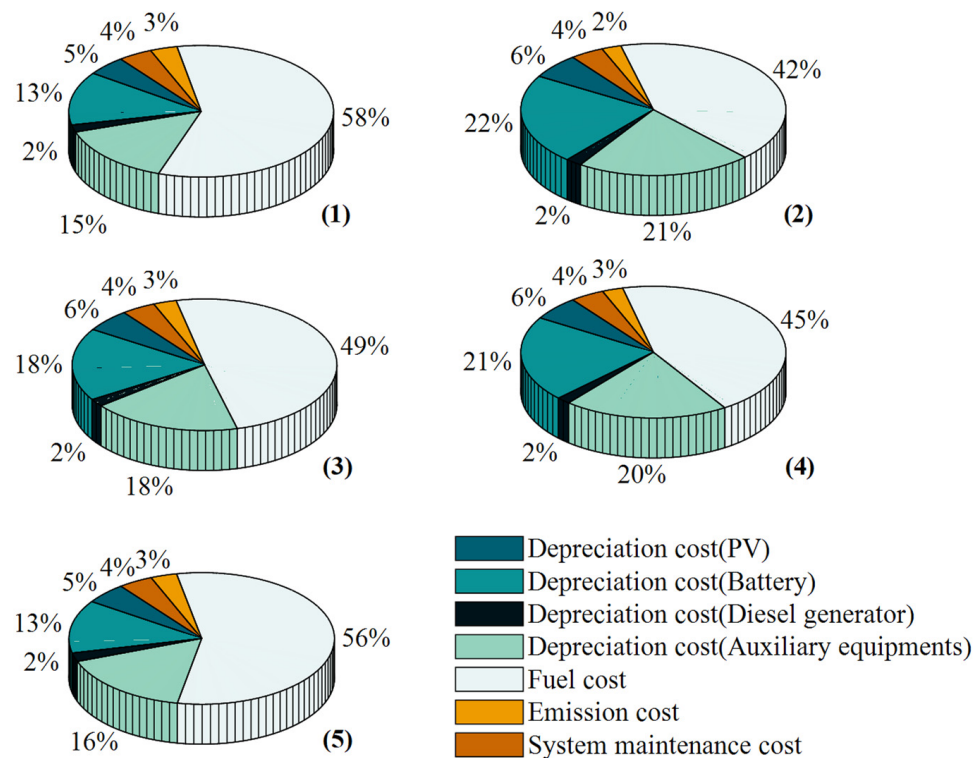
The obtained 1000 sets of optimal sizes are only used for the respective radiation scenarios to acquire the minimum COE by optimal energy scheduling. However, the range of optimal sizes obtained for each component in the optimal design, with sufficient radiation scenarios, provides a reference for sizing configurations of systems under radiation uncertainty. In this section, five candidate sizes are selected from the optimal range, while the techno-economic analysis is performed based on the remaining 1000 sets of radiation scenarios. Respectively, sizes (1), (2), and (3) are the minimum, maximum, and mean sizes from the optimal size range of each component, and sizes (4) and (5) are the optimal sizes of the maximum/minimum yearly total radiation scenario.

Table 4 gives the statistical index for each size of the HES, including the specific size information, initial capital cost, annual COE, average energy supply, average PV power generation, etc. Overall, the main difference between the various size combinations comes from the battery capacity, which also creates a gap in their initial investment. The annual COE fluctuated within USD 0.0157 to 0.0194/kWh for each HES in the random scenario, with a difference of USD 0.0284/kWh between the maximum and minimum COE for all HES. The smallest COE occurs at the size (5) of USD 0.3821/kWh, and since it is taken from the smallest yearly total radiation scenario, a larger diesel generator capacity must be configured to meet the load demand. The largest COE occurs under size (2), with USD 0.4105/kWh; the size consists of the maximum sizes from the optimal size range of each component, leading to the highest initial capital cost of USD 6909.8. Only size (1) shows a loss of energy supply, with a yearly average of 12.03 kWh and a loss probability of 0.15%. The average proportion of PV generation is positively correlated to its capacity, with a maximum of 64.1% for size (2), while the average curtailment rate is correlated to battery capacity, with a minimum of 13.17% for size (4) (752.17kWh/year). Size (4) is the most notable among all candidate size combinations, with average COE of USD 0.3931/kWh, which is only USD 0.0041/kWh higher than the minimum, yet it exhibits the second-highest PV proportion and the smallest curtailment rate.

Specifically, the COE composition for each size of HES is shown in Figure 10. The fuel and emission costs of diesel generators comprise the largest share for each size combination, followed by the depreciation cost of auxiliary equipment, which is directly related to the initial capital cost of the system. The depreciation cost of the PV and diesel generators is not sensitive to the HES size, while the depreciation cost of the battery shows a significant increase with the increase in battery capacity. Meanwhile, higher battery depreciation costs mean that the battery meets the flexible take-up of PV power through more frequent charging and discharging, which reduces the fuel costs of the diesel generator. The main advantage of distributed HES is the flexibility to meet the load demand, as well to express the environmental friendliness of the renewable energy it contains. The COE composition of both size (2) and size (4) exhibit high battery depreciation costs and low fuel costs, echoing the high PV proportion of both in Table 4. Nevertheless, size (4) is better than size (2) in terms of the cost of the initial investment, the COE, and the PV curtailment rate, and seems to be the best choice in terms of both economic and environmental considerations.

**Table 4.** Statistical results of chosen size combination.

Parameter	Description	(1)	(2)	(3)	(4)	(5)
Yearly total radiation (kW/m <sup>2</sup> )	Min.	1590.0				
	Max.	1894.8				
	Mean	1746.0				
	Range	304.8				
Size	PV (m <sup>2</sup> )	10.58	13.86	12.37	13.07	11.25
	Battery (kWh)	7.27	15.1	11.27	14.51	7.98
	Diesel generator (kW)	1.54	2.23	1.84	1.67	2.09
Initial capital (USD)	Total	4483.6	6909.8	5806.3	6377.0	5142.8
	PV	3018.5	3954.3	3529.2	3728.9	3209.6
	Battery	986.6	2050.6	1530.5	1970.5	1083.8
	Diesel generator	626.6	905.0	746.7	677.7	849.4
COE (USD/kWh)	Min.	0.3822	0.3911	0.3856	0.3842	0.3821
	Max.	0.4013	0.4105	0.4035	0.4053	0.3978
	Mean	0.3908	0.3996	0.3933	0.3931	0.389
	Range	0.0191	0.0194	0.0179	0.0211	0.0157
Power supply (Mean)	Loss (kWh)	12.03	0	0	0	0
	Loss probability (%)	0.15	0	0	0	0
PV Power (Mean)	Curtailment (kWh)	933.03	880.47	916.83	752.17	1034.8
	Curtailment Rate (%)	20.19	14.54	16.97	13.17	21.06
	Proportion (%)	45.7	64.1	55.59	61.42	48.06



**Figure 10.** Proportion of COE compositions for sizes (1)–(5). (1) PV-10.58 m<sup>2</sup>, battery-7.27 kWh, diesel generator-1.54 kW; (2) PV-13.86 m<sup>2</sup>, battery-15.1 kWh, diesel generator-2.23 kW; (3) PV-12.37 m<sup>2</sup>, battery-11.27 kWh, diesel generator-1.84 kW; (4) PV-13.07 m<sup>2</sup>, battery-14.51 kWh, diesel generator-1.67 kW; (5) PV-11.25 m<sup>2</sup>, battery-7.98 kWh, diesel generator-2.09 kW.

### 5. Conclusions

A novel method for the stochastic modeling of solar radiation is proposed, with consideration of both intraday variation and daily stochastic evolution. By introducing the

clearness index, the daily radiation intensity is divided into nine states, and the evolution characteristics are modeled based on the Markov model. Diffusion-based kernel density estimation is used to obtain the probabilistic distributions of the intraday clearness index at different daily clearness states. The use of the clear sky radiation model naturally ensures that the obtained radiation data comply with the local solar seasonality and variations in sunlight duration. Meanwhile, the two-layer stochastic model ensures the rationality of daily variations and intraday fluctuations in radiation intensity, providing a data foundation for the optimization of the designing of solar-powered hybrid energy systems. A methodology for the application of the proposed stochastic radiation model is illustrated by optimal sizing in the case of a solar-powered hybrid energy system. The main conclusions are presented below.

- (1) The proposed generation model can effectively reflect variations in solar radiation, providing a reliable data foundation for the optimization of the designing of solar-powered hybrid energy systems (HES).
- (2) The optimal size range for each device in the hybrid energy system under random solar radiation variations can be obtained based on the proposed model.
- (3) The size combination in the maximum total yearly radiation scenario exhibits a better overall performance. Compared to the worst-case scenario, its PV curtailment rate decreases by 7.02%, and the COE is only USD 0.0041/kWh higher than the current minimum.

This work considers a simple off-grid PV-battery-diesel generator system, but it can be easily extended to more complex architectures, including other renewable energy sources and grid connections.

**Author Contributions:** Conceptualization, D.L.; Methodology, L.M. and Y.L. (Yiping Luo); Software, L.M.; Validation, P.W.; Investigation, P.W.; Data curation, Y.L. (Yuanxia Li); Writing—original draft, D.L.; Writing—review & editing, Y.L. (Yiping Luo); Supervision, Y.L. (Yuanxia Li). All authors have read and agreed to the published version of the manuscript.

**Funding:** This work was supported by the China Postdoctoral Science Foundation (No. 2020M683526).

**Data Availability Statement:** Data are contained within the article.

**Conflicts of Interest:** D.L., L.M., P.W. and Y.L. (Yuanxia Li) were employed by State Grid Gansu Electric Power Company Linxia Power Supply Company. The remaining authors declare that the research was conducted in the absence of any commercial or financial relationships that could be construed as a potential conflict of interest.

## References

1. Fodstad, M.; del Granado, P.C.; Hellemo, L.; Knudsen, B.R.; Pisciella, P.; Silvast, A.; Bordin, C.; Schmidt, S.; Straus, J. Next frontiers in energy system modelling: A review on challenges and the state of the art. *Renew. Sustain. Energy Rev.* **2022**, *160*, 112246. [[CrossRef](#)]
2. Yoro, K.O.; Daramola, M.O.; Sekoai, P.T.; Wilson, U.N.; Eterigho-Ikelegbe, O. Update on current approaches, challenges, and prospects of modeling and simulation in renewable and sustainable energy systems. *Renew. Sustain. Energy Rev.* **2021**, *150*, 111506. [[CrossRef](#)]
3. Sorrenti, I.; Rasmussen TB, H.; You, S.; Wu, Q. The role of power-to-X in hybrid renewable energy systems: A comprehensive review. *Renew. Sustain. Energy Rev.* **2022**, *165*, 112380. [[CrossRef](#)]
4. Niknam, T.; Azizipanah-Abarghooee, R.; Narimani, M.R. An efficient scenario-based stochastic programming framework for multi-objective optimal micro-grid operation. *Appl. Energy* **2012**, *99*, 455–470. [[CrossRef](#)]
5. Temiz, M.; Dincer, I. Development of solar and wind based hydrogen energy systems for sustainable communities. *Energy Convers. Manag.* **2022**, *269*, 116090. [[CrossRef](#)]
6. Zhang, C.; Xia, J.; Guo, X.; Huang, C.; Lin, P.; Zhang, X. Multi-optimal design and dispatch for a grid-connected solar photovoltaic-based multigeneration energy system through economic, energy and environmental assessment. *Sol. Energy* **2022**, *243*, 393–409. [[CrossRef](#)]
7. Chen, Z.; Xie, Y.L.; Zhang, H.X.; Gu, Y.J.; Zhang, X.W. Optimal design and performance assessment for a solar powered electricity, heating and hydrogen integrated energy system. *Energy* **2023**, *262*, 125453. [[CrossRef](#)]
8. El-Baz, W.; Tzschentschler, P.; Wagner, U. Day-ahead probabilistic PV generation forecast for buildings energy management systems. *Sol. Energy* **2018**, *171*, 478–490. [[CrossRef](#)]

9. Lasemi, M.A.; Arabkoohsar, A.; Hajizadeh, A.; Mohammadi-Ivatloo, B. A comprehensive review on optimization challenges of smart energy hubs under uncertainty factors. *Renew. Sustain. Energy Rev.* **2022**, *160*, 112320. [[CrossRef](#)]
10. Rauf, A.; Kassas, M.; Khalid, M. Data-driven optimal battery storage sizing for grid-connected hybrid distributed generations considering solar and wind uncertainty. *Sustainability* **2022**, *14*, 11002. [[CrossRef](#)]
11. Guo, X.; Zhang, S.; Wang, D.; Peng, N.; Zhang, X. Techno-economic feasibility study of an electric-thermal coupling integrated energy system for commercial buildings in different latitudes. *Int. J. Energy Res.* **2020**, *44*, 7789–7806. [[CrossRef](#)]
12. Zhang, X.; Li, M.; Ge, Y.; Li, G. Techno-economic feasibility analysis of solar photovoltaic power generation for buildings. *App. Therm. Eng.* **2016**, *108*, 1362–1371. [[CrossRef](#)]
13. Li, M.; Zhang, X.; Li, G.; Jiang, C. A feasibility study of microgrids for reducing energy use and GHG emissions in an industrial application. *Appl. Energy* **2016**, *176*, 138–148. [[CrossRef](#)]
14. Güven, A.F.; Yörükeren, N.; Samy, M.M. Design optimization of a stand-alone green energy system of university campus based on Jaya-Harmony Search and Ant Colony Optimization algorithms approaches. *Energy* **2022**, *253*, 124089. [[CrossRef](#)]
15. Schuster, C.S. Analytical framework for the assessment and modelling of multi-junction solar cells in the outdoors. *Renew. Energy* **2020**, *152*, 1367–1379. [[CrossRef](#)]
16. Hassan, Q.; Algburi, S.; Sameen, A.Z.; Salman, H.M.; Jaszczur, M. A review of hybrid renewable energy systems: Solar and wind-powered solutions: Challenges, opportunities, and policy implications. *Results Eng.* **2023**, *20*, 101621. [[CrossRef](#)]
17. Di Somma, M.; Graditi, G.; Heydarian-Forushani, E.; Shafie-khah, M.; Siano, P. Stochastic optimal scheduling of distributed energy resources with renewables considering economic and environmental aspects. *Renew. Energy* **2018**, *116*, 272–287. [[CrossRef](#)]
18. Li, H.; Zhao, J.; Li, M.; Zhong, S.; Wang, F.; He, F.; Zhu, J. Determining the economic design radiation for a solar heating system through uncertainty analysis. *Sol. Energy* **2020**, *195*, 54–63. [[CrossRef](#)]
19. Cho, D.; Valenzuela, J. A scenario-based optimization model for determining the capacity of a residential off-grid PV-battery system. *Sol. Energy* **2022**, *233*, 478–488. [[CrossRef](#)]
20. Liu, Z.; Cui, Y.; Wang, J.; Yue, C.; Agbodjan, Y.S.; Yang, Y. Multi-objective optimization of multi-energy complementary integrated energy systems considering load prediction and renewable energy production uncertainties. *Energy* **2022**, *254*, 124399. [[CrossRef](#)]
21. Biencinto, M.; González, L.; Valenzuela, L. Using time-windowed solar radiation profiles to assess the daily uncertainty of solar thermal electricity production forecasts. *J. Clean. Prod.* **2022**, *379*, 134821. [[CrossRef](#)]
22. Zhang, X. A statistical approach for sub-hourly solar radiation reconstruction. *Renew. Energy* **2014**, *71*, 307–314. [[CrossRef](#)]
23. Hocaoglu, F.O. Stochastic approach for daily solar radiation modeling. *Sol. Energy* **2011**, *85*, 278–287. [[CrossRef](#)]
24. Torres, J.L.; de Blas, M.; Torres, L.M.; García, A.; de Francisco, A. Synthetic generation of standard sky types series using Markov Transition Matrices. *Renew. Energy* **2014**, *62*, 731–736. [[CrossRef](#)]
25. Ngoko, B.O.; Sugihara, H.; Funaki, T. Synthetic generation of high temporal resolution solar radiation data using Markov models. *Sol. Energy* **2014**, *103*, 160–170. [[CrossRef](#)]
26. Bouabdallah, A.; Olivier, J.C.; Bourguet, S.; Machmoum, M.; Schaeffer, E. Safe sizing methodology applied to a standalone photovoltaic system. *Renew. Energy* **2015**, *80*, 266–274. [[CrossRef](#)]
27. Pauluhn, A.; Huber, M.C.E.; Smith, P.L.; Colina, L. Spectroradiometry with space telescopes. *Astron. Astrophys. Rev.* **2015**, *24*, 3. [[CrossRef](#)]
28. Bouabdallah, A.; Bourguet, S.; Olivier, J.C.; Machmoum, M. Photovoltaic energy for the fixed and tracking system based on the modeling of solar radiation. In Proceedings of the IECON 2013-39th Annual Conference of the IEEE Industrial Electronics Society, Vienna, Austria, 10–13 November 2013; pp. 1821–1826. [[CrossRef](#)]
29. Duffie, J.A.; Beckman, W.A. *Solar Engineering of Thermal Processes*, 4th ed.; John Wiley & Sons, Inc.: Hoboken, NJ, USA, 2013.
30. Reindl, D.T.; Beckman, W.A.; Duffie, J.A. Evaluation of hourly tilted surface radiation models. *Sol. Energy* **1990**, *45*, 9–17. [[CrossRef](#)]
31. Loutzenhiser, P.G.; Manz, H.; Felsmann, C.; Strachan, P.A.; Frank, T.H.; Maxwell, G.M. Empirical validation of models to compute solar radiation on inclined surfaces for building energy simulation. *Sol. Energy* **2007**, *81*, 254–267. [[CrossRef](#)]
32. Carpinone, A.; Giorgio, M.; Langella, R.; Testa, A. Markov chain modeling for very-short-term wind power forecasting. *Electr. Power Syst. Res.* **2015**, *122*, 152–158. [[CrossRef](#)]
33. Che, Y.; Wang, X.; Lv, X.; Hu, Y.; Teng, Y. Study on probability distribution of electrified railway traction loads based on kernel density estimator via diffusion. *Int. J. Electr. Power Energy Syst.* **2019**, *106*, 383–391. [[CrossRef](#)]
34. Qin, Z.; Li, W.; Xiong, X. Estimating wind speed probability distribution using kernel density method. *Electr. Power Syst. Res.* **2011**, *81*, 2139–2146. [[CrossRef](#)]
35. Botev, Z.I.; Grotowski, J.F.; Kroese, D.P. Kernel density estimation via diffusion. *Ann. Stat.* **2010**, *38*, 2916–2957. [[CrossRef](#)]
36. Seger, P.V.H.; Rigo-Mariani, R.; Thivel, P.X.; Riu, D. A storage degradation model of Li-ion batteries to integrate ageing effects in the optimal management and design of an isolated microgrid. *Appl. Energy* **2023**, *333*, 120584. [[CrossRef](#)]

**Disclaimer/Publisher’s Note:** The statements, opinions and data contained in all publications are solely those of the individual author(s) and contributor(s) and not of MDPI and/or the editor(s). MDPI and/or the editor(s) disclaim responsibility for any injury to people or property resulting from any ideas, methods, instructions or products referred to in the content.